ARMY RESEARCH LABORATORY

Analysis of a Novel Fracture Toughness Testing Geometry

by Bryan M. Love

ARL-TR-6266 **December 2012**

NOTICES

Disclaimers

The findings in this report are not to be construed as an official Department of the Army position unless so designated by other authorized documents.

Citation of manufacturer's or trade names does not constitute an official endorsement or approval of the use thereof.

Destroy this report when it is no longer needed. Do not return it to the originator.

Army Research Laboratory
Aberdeen Proving Ground, MD 21005-5069

ARL-TR-6266 **December 2012**

Analysis of a Novel Fracture Toughness Testing Geometry

Bryan M. Love
Weapons and Materials Research Directorate, ARL

REPORT DOCUMENTATION PAGE	Form Approved OMB No. 0704-0188

1. REPORT DATE *(DD-MM-YYYY)*	2. REPORT TYPE	3. DATES COVERED (From - To)
December 2012	Final	February 2012–July 2012

4. TITLE AND SUBTITLE
Analysis of a Novel Fracture Toughness Testing Geometry

5a. CONTRACT NUMBER

5b. GRANT NUMBER

5c. PROGRAM ELEMENT NUMBER

6. AUTHOR(S)
Bryan M. Love

5d. PROJECT NUMBER
H42

5e. TASK NUMBER

5f. WORK UNIT NUMBER

7. PERFORMING ORGANIZATION NAME(S) AND ADDRESS(ES)
U.S. Army Research Laboratory
ATTN: RDRL-WMM-B
Aberdeen Proving Ground, MD 21005-5069

8. PERFORMING ORGANIZATION REPORT NUMBER
ARL-TR-6266

9. SPONSORING/MONITORING AGENCY NAME(S) AND ADDRESS(ES)

10. SPONSOR/MONITOR'S ACRONYM(S)

11. SPONSOR/MONITOR'S REPORT NUMBER(S)

12. DISTRIBUTION/AVAILABILITY STATEMENT
Approved for public release; distribution is unlimited.

13. SUPPLEMENTARY NOTES

14. ABSTRACT

Computational analyses were conducted on novel fracture toughness specimens known as "butterfly" specimens, which were developed at the U.S. Army Research Laboratory. A three-dimensional (3-D), J-integral technique was established and validated against published results for a simple geometry. The technique was then used to generate a stress intensity factor function for a range of geometries for the butterfly specimen. A displacement-based description of the load on the specimen was developed that removes the need to accurately determine the specimen/platen frictional effects, and 3-D analyses were conducted to elucidate specimen thickness effects and their implications on surface measurements that are taken during experimental studies.

15. SUBJECT TERMS
fracture toughness, stress intensity factor, computational modeling, high rate loading, experimental methodology

16. SECURITY CLASSIFICATION OF:			17. LIMITATION OF ABSTRACT	18. NUMBER OF PAGES	19a. NAME OF RESPONSIBLE PERSON
a. REPORT	b. ABSTRACT	c. THIS PAGE			Bryan M. Love
Unclassified	Unclassified	Unclassified	UU	28	19b. TELEPHONE NUMBER (*Include area code*) 410-306-1949

Standard Form 298 (Rev. 8/98)
Prescribed by ANSI Std. Z39.18

Contents

List of Figures

List of Tables

INTENTIONALLY LEFT BLANK.

1. Introduction

Recently, Syn and Chen (*1*) utilized a small fracture specimen to study the fracture behavior of an aluminum/epoxy interface under high rate loading. The specimen, due to its novel shape, is frequently referred to as a "butterfly" specimen, as it mimics a compact four-point bend specimen, with suitable dimensions for high strain-rate testing in a Kolsky bar. Whittie et al. (*2*) utilized a butterfly specimen to examine the fracture toughness of cross-linked epoxies as a function of loading rate; the small specimen allowed both servo-hydraulic and Kolsky bar testing. The specimen geometry was further developed by Weerasooriya et al. (*3*) to study fracture behavior of adhesive bonds at low and high rates of loading. The combined research (*1–3*) allowed determination of fracture energies by examining the load-displacement curve from either the servo-hydraulic tester or through traditional split Hopkinson pressure bar (SHPB) bar analysis. However, measurement of fracture toughness through crack-tip opening displacements or local strain fields was well outside of the digital image correlation (DIC) system's resolution (*2, 3*), as the epoxies and adhesives considered were quite brittle and displacements near the crack-tip are on the order of 10 μm. Stress intensity factor solutions for butterfly specimens are not available in the literature, preventing comparison of the measured fracture energies with the expected stress intensity factors at the crack-tip.

In this work, we sought to derive a stress intensity factor solution for a generalized version of the U.S. Army Research Laboratory (ARL) butterfly specimen within the useful range of geometries for Kolsky bar use. The linear elastic stress intensity factor solution that has been investigated in this study is the starting point to allow more advanced analysis of viscoelastic, strain-rate, and temperature effects that are critically important for many polymeric materials.

2. Methodology

The finite element method is widely used to calculate stress intensity factors for various geometries that cannot be computed analytically. We utilized Sandia National Laboratories' Sierra suite of finite element codes (*4*) to perform quasi-static, implicit solid dynamics, and explicit solid dynamics analyses. The use of Sierra and Department of Defense high-performance computing assets allowed the completion of a multitude of fully three-dimensional (3-D) simulations to explore the effects of specimen geometry, loading magnitudes and rates, frictional effects, and numerical resolution on the stress intensity factor.

Computation of the stress intensity factor from finite element results was performed using the J-integral (*5*). While the J-integral has documented path-dependence for elastic-plastic materials (particularly in the plastic zone) (*6*), the integral is path-independent for the linear and nonlinear elastic materials considered here. This path independence allows the J-integral to be a robust calculation of the stress intensity factor, as it does not rely on the numerical solution accurately capturing the singularity at the crack-tip. The J-integral is defined in two dimensions (2-D) as

$$J = \oint_{\Gamma} (W n_1 - \sigma_{ji} n_j u_{i,1}) d\Gamma \ , \tag{1}$$

where Γ represents a closed path around the crack-tip, n is the outward normal to Γ, W is the strain energy density, σ is the Cauchy stress, and u is the displacement. Note that in equation 1, the 1-direction is taken to be along the path of the crack. To evaluate J, the domain integral method (*5*) is utilized:

$$J_Q = -\int_A (W q_{,1} - \sigma_{ji} q_{,j} u_{i,1}) dA. \tag{2}$$

In equation 2, A is a domain that contains both crack faces as part of the boundary, and the function q is defined such that $q = 1$ on the inner boundary of A and $q = 0$ on the outer boundary. Li et al. (*5*) demonstrated that $J = J_Q$ for nonlinear elastic materials; for inelastic materials, J_Q is an average value of J over paths determined by curves of constant q in the domain (*7*). This domain integral can be evaluated using standard finite element techniques. In this work, the function q was taken from Carka and Landis (*7*):

$$q = \frac{r - R_o}{R_o - R_i}, \tag{3}$$

where r is a radial coordinate centered on the crack-tip and R_i and R_o represent the inner and outer radii of the annular domain A.

To test the efficacy of the numerical simulation, an edge-cracked plate loaded in simple tension was simulated in Sierra using a plane strain assumption. The plate, with in-plane dimensions of $H = 20$ mm and $W = 10$ mm, was simulated with edge cracks of lengths $a = 1$, 2, and 3 mm. Meshes of uniform quadrilateral elements of side lengths $a/5$, $a/15$, and $a/45$ were utilized. The J-integral was evaluated, as described previously, using the domain integral for a variety of radii ranging from $a/10$ to $2a$, and all deviated less than 0.5%, thus verifying path independence. Recalling that, for a linear elastic material under plane strain deformations, the stress intensity factor is related to the J-integral by

$$K = \sqrt{\frac{E}{1 - \nu^2} J}, \tag{4}$$

one can compare the J-integral results to published values for the stress intensity factor. Tada et al. (*8*) give an empirical form for the stress intensity factor of an edge-cracked plate under simple tension (to a claimed 0.5% accuracy) of

$$K_I = \sigma\sqrt{\pi a}\left(1.122 - 0.231\left(\frac{a}{b}\right) + 10.556\left(\frac{a}{b}\right)^2 - 21.710\left(\frac{a}{b}\right)^3 + 30.382\left(\frac{a}{b}\right)^4\right), \tag{5}$$

with a representing the crack length and b representing the plate width. For the scenario with a = 2 mm and b = 10 mm, the finite-element results for the three mesh resolutions are given in table 1. Note the excellent agreement with the published results for the a/15 and a/45 cases. Further meshing trials indicated that this mesh resolution needs only to be maintained in a small area around the crack-tip, dramatically reducing the number of elements needed for simulation.

Table 1. Stress intensity factors for various mesh resolutions.

Mesh Resolution	**Calculated $K_I/(\sigma^*(\pi a)^{0.5})$**	**Error (%)**
a/5	1.445	5.29
a/15	1.367	–0.44
a/45	1.360	–0.93

In addition to the quasi-static plane strain case, fully 3-D dynamic simulations were conducted to determine the efficacy of using the explicit solver to find stress intensity factors. The dynamic effects were analyzed by evaluating the dynamic J-integral (adding the kinetic energy to the strain energy term in equation 1) as a function of time. Monitoring the individual terms allows evaluation of the inertial contributions and time fluctuations. For ramp loads or pulse-to-plateau loadings of sufficiently slow rates, the contribution of the dynamic term is negligible and the low strain-rate simulation results are within numerical error of the quasi-static analytical results. The effects of a 3-D specimen are subtle for the problem studied here; the thickness of the specimen will determine if the results are closer to plane stress or plane strain. Giner et al. (*9*) express a path-area independent integral J_{x1} as

$$J_{x1} = J_P + J_A = \oint_\Gamma \left(W n_1 - \sigma_{ij}\frac{\partial u_j}{\partial x_1} n_i\right) d\Gamma - \int_{A(\Gamma)} \frac{\partial}{\partial x_3}\left(\sigma_{i3}\frac{\partial u_i}{\partial x_1}\right) dA. \tag{6}$$

Here, J_P is the standard line integral used in the 2-D J-integral with path Γ, and J_A is an integral of out-of-plane stresses over the area $A(\Gamma)$ contained by Γ. Note that J_{x1} is evaluated for a position along the crack-tip. Giner et al. (*9*) note that J_P and J_A are a function of the position relative to the boundaries and that J_A vanishes for infinitesimal Γ. J_P can be evaluated using the domain integral method (equation 2). J_A is evaluated as an area integral inside the surface bounded by q = 0, with the integration weighted by q (thus giving an average for $R_i < r < R_o$, for the q in equation 3). For the edge-cracked plate with H = W = 10 mm and a = 2 mm, J_{x1} was calculated along the thickness direction for specimen thicknesses of 1, 5, 10, 20, and 50 mm;

results are plotted normalized by the thickness D in figure 1. The centerline value of J_{x1} transitions from values close to the plane stress value of J at D = 1 and 5 mm to values close to the plane strain value at D = 20 mm. Also note that there are distinct differences between the edges of specimens and the centerline, which should be considered when conducting analyses on surface-based measurements. That said, utilizing the explicit solver on a 3-D problem, with sufficiently slow loading and long analysis times, reproduces theoretical results for two dimensions. The ability to utilize the explicit solver allows a common numerical framework to be used for the quasi-static testing in this report to the planned high strain-rate simulations, similar to prior experiments (*1–3*).

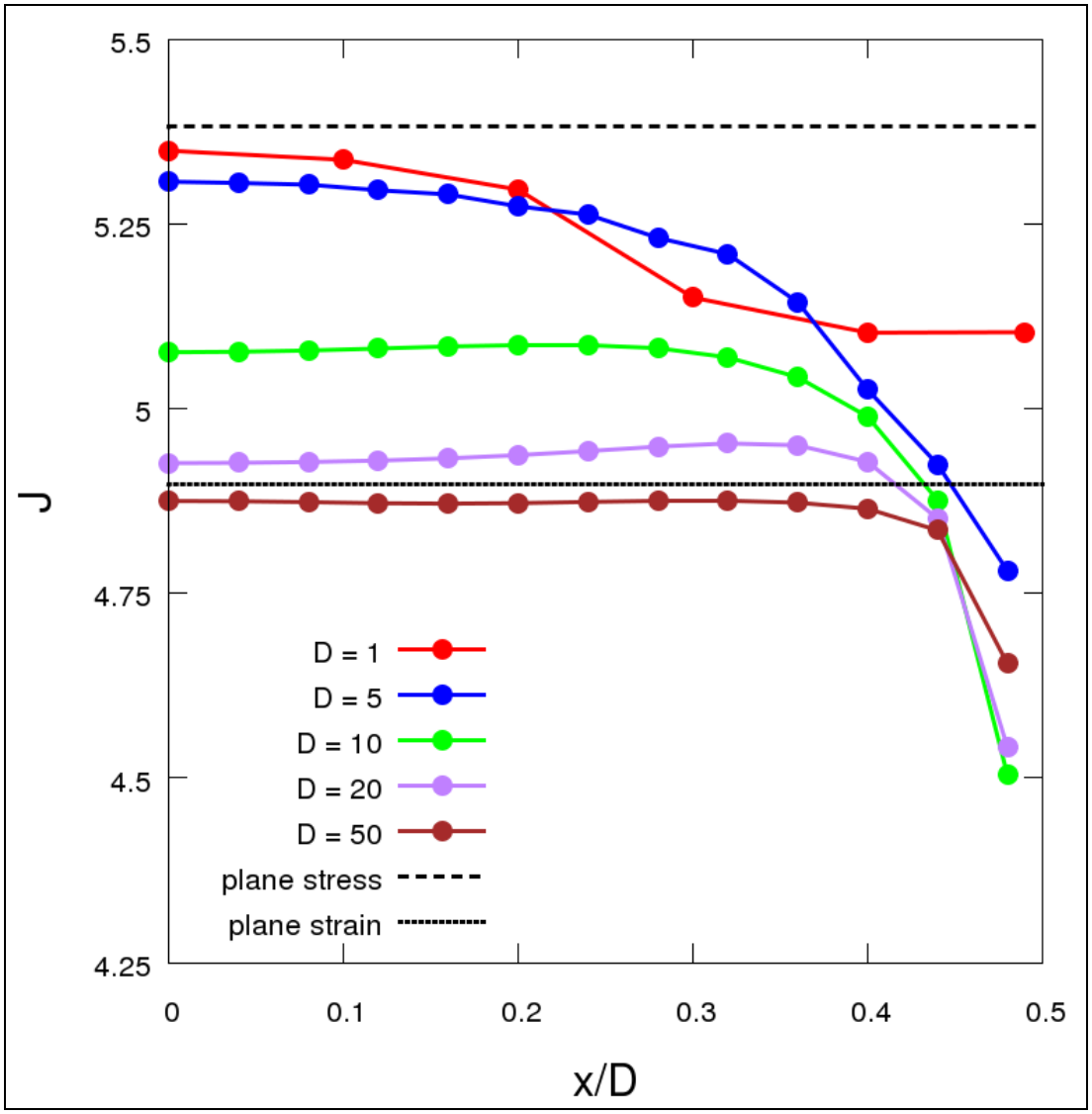

Figure 1. J_{x1} as a function of axial-coordinate for edge-cracked specimens of thicknesses 1, 5, 10, 20, and 50 mm.

3. ARL Butterfly Specimen

While the experimental measurement of displacement and force gives overall fracture energy, it does so in a specific configuration that is not readily generalized. Prior research into similar geometries (*1*) utilizes the stress intensity factor for a four-point bending specimen without testing its efficacy for this particular nonstandard geometry. We sought to find a more accurate representation of the stress intensity factor, parameterized for a generalized version of this geometry, utilizing the finite element method.

Shown in figure 2, the generalized version of this geometry has the following parameters: an overall height H and thickness D, normal distance from the centerline to the upper contact point L_1, normal distance from the centerline to the upper contact point L_2, crack root distance a_0, and overall crack length a. Note that the radii of the upper and lower contact surfaces are equal to L_1.

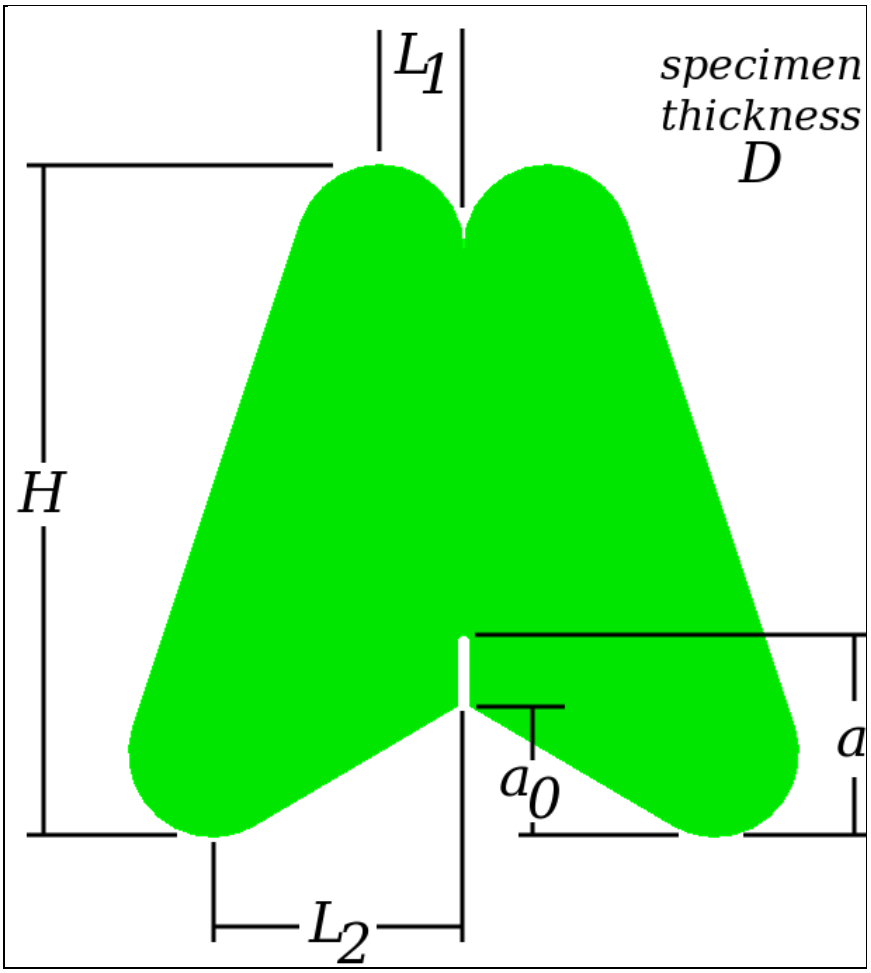

Figure 2. Generalized geometry for butterfly bending specimen.

3.1 Numerical Setup for Butterfly Specimen

The butterfly specimen was developed as a simple way to produce a mode-I crack utilizing displacement-controlled compression tests, particularly for high strain-rate loading. Here, the effort was to characterize the fracture toughness of a brittle epoxy with a stiffness of 2.2 GPa and Poisson's ratio of 0.3. Numerically, we examined the compression of a 20-mm-deep (D) specimen with metallic platens 25 mm in diameter and 6.35 mm thick. Recognizable factors that are not based on the specimen geometry and displacement amplitude arise in the numerical simulations: mesh resolution, loading history, platen material, and frictional effects. To ascertain the effects of these factors, a standard geometry was selected (L_1 = 1.7 mm; L_2 = 4.15 mm; H = 13.49 mm; a_0 = 2.97 mm; a = 4.1 mm; crack is 0.3 mm wide with a rounded nose) and a set of parametric studies was conducted.

Initial simulations were conducted with steel (E = 200 GPa; ν = 0.29) platens with a Coulomb friction coefficient of 0.001 on the standard geometry. It was found that a small friction coefficient was necessary to prevent small asymmetries from causing significant slip. The specimen was meshed with a near-uniform mesh resolution, then refined near the crack-tip and the contact areas on both the specimen and platen (in the form of a 3:1 reduction in element side length), as shown in figure 3. It was found that the contact patches needed a certain level of refinement to prevent slip-stick issues for larger values of the friction coefficients. To ascertain the effect of loading amplitude on the result, the standard specimen meshed with a resolution of 0.6 mm was subjected to a displacement-controlled ramp loading from 0 to 1.0 mm of displacement in 10 ms. Computation of J_{x1} on the center-plane of the specimen was conducted at various times in the simulation, and the load applied to the platens was computed by integrating the normal stresses over the platen surfaces. It was found that the applied load was proportional to the square root of J_{x1}; or, in other words, the load is proportional to the stress intensity factor, as shown in figure 4.

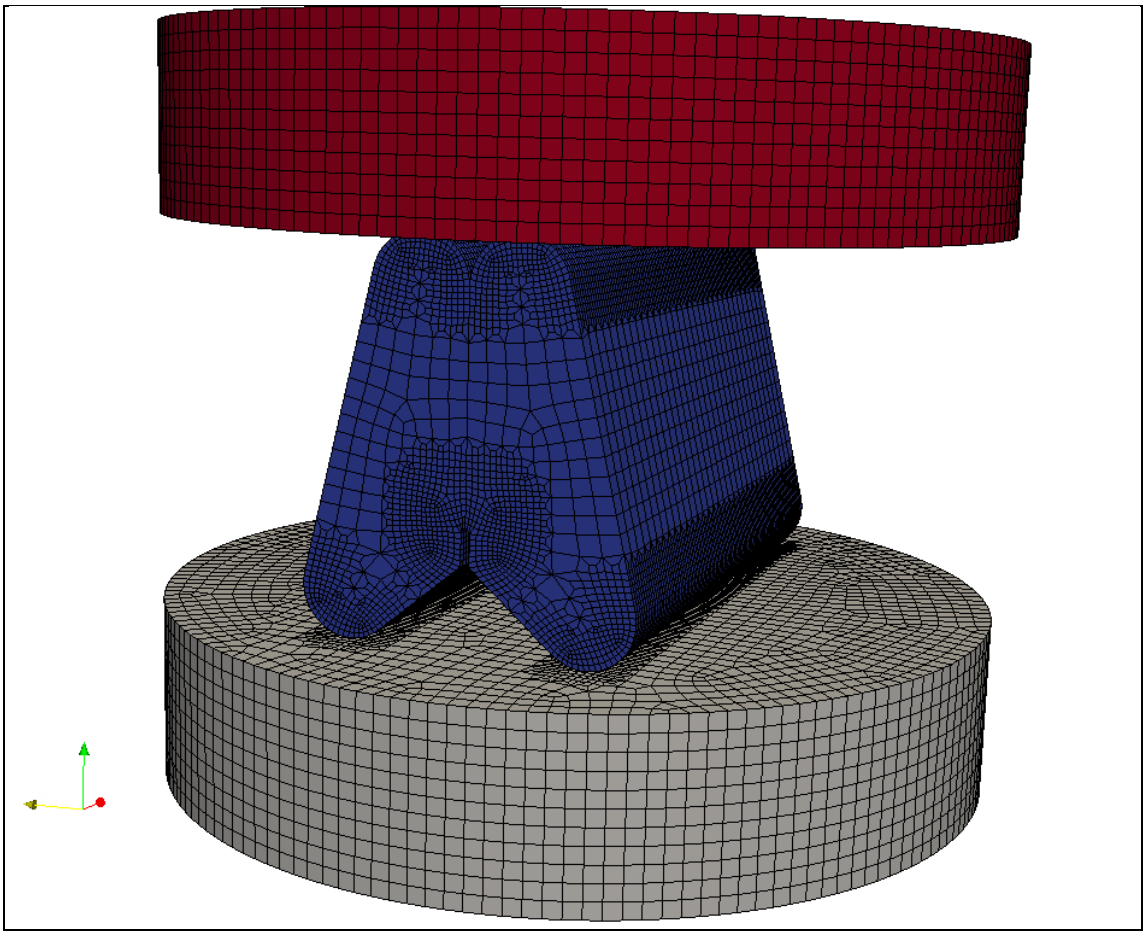

Figure 3. Sample mesh for mesh resolution studies.

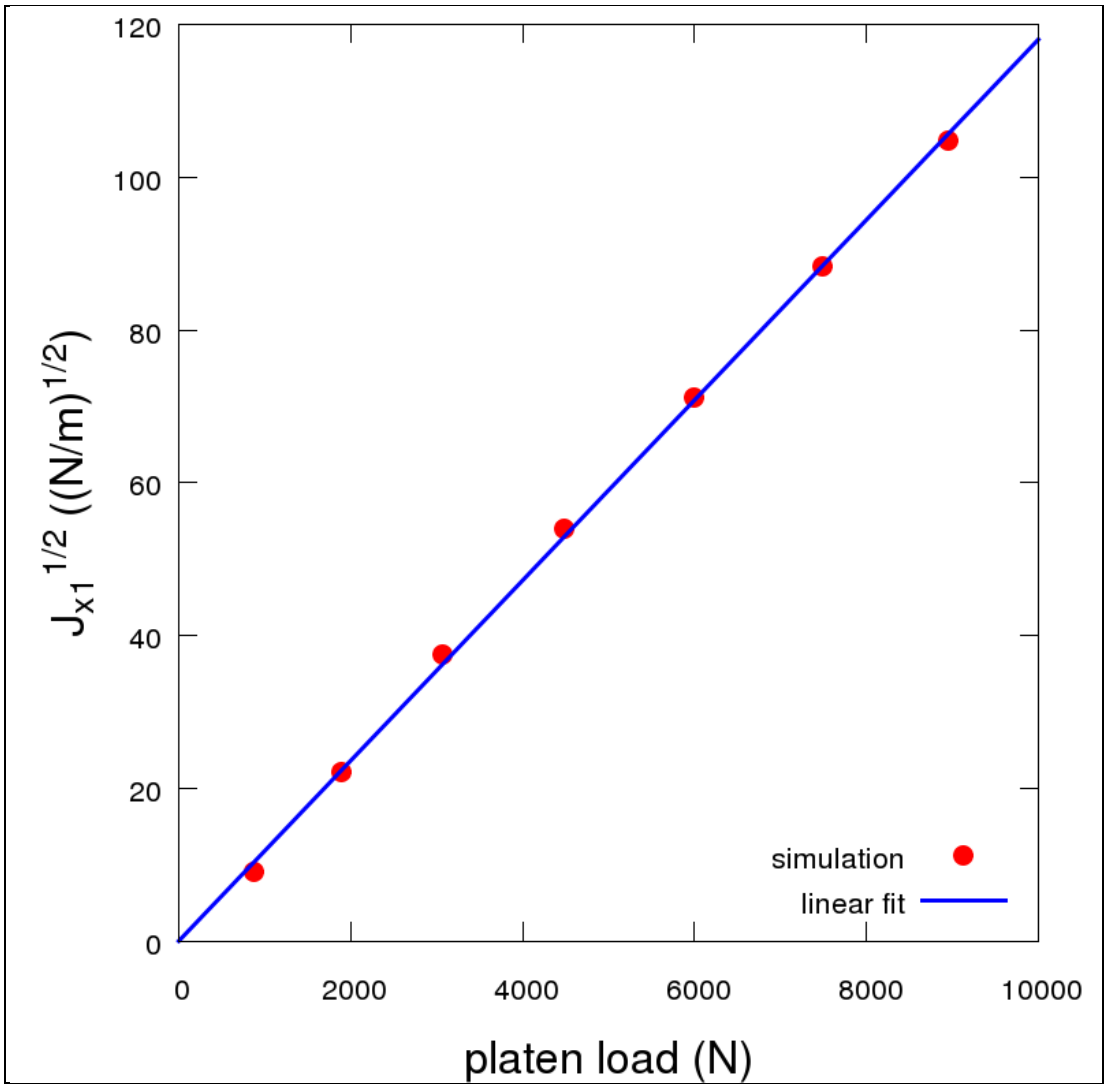

Figure 4. Square root of J_{x1} vs. applied load for the standard butterfly specimen.

A mesh resolution study was conducted to insure convergence in J_{x1} before pursuing further parametric studies. The lower platen was held fixed in the loading direction, with the upper platen given a constant velocity of 0.1 m/s. Thus, the standard mesh shown in figure 3 was refined by splitting each node-to-node segment in half (thus producing double the mesh density). Results are shown in figure 5. There is less than a 2% difference between the $J_{x1}^{1/2}$ profiles at a given platen displacement, echoing the results from the edge-cracked tension specimen in section 3.1 (and an attribute of the nonlocal nature of the J-integral). This differential is even smaller when the results are normalized for a common load or tip displacement. Further analyses in this report are conducted with a mesh resolution of 0.6 mm (overall)/0.2 mm (near crack-tip).

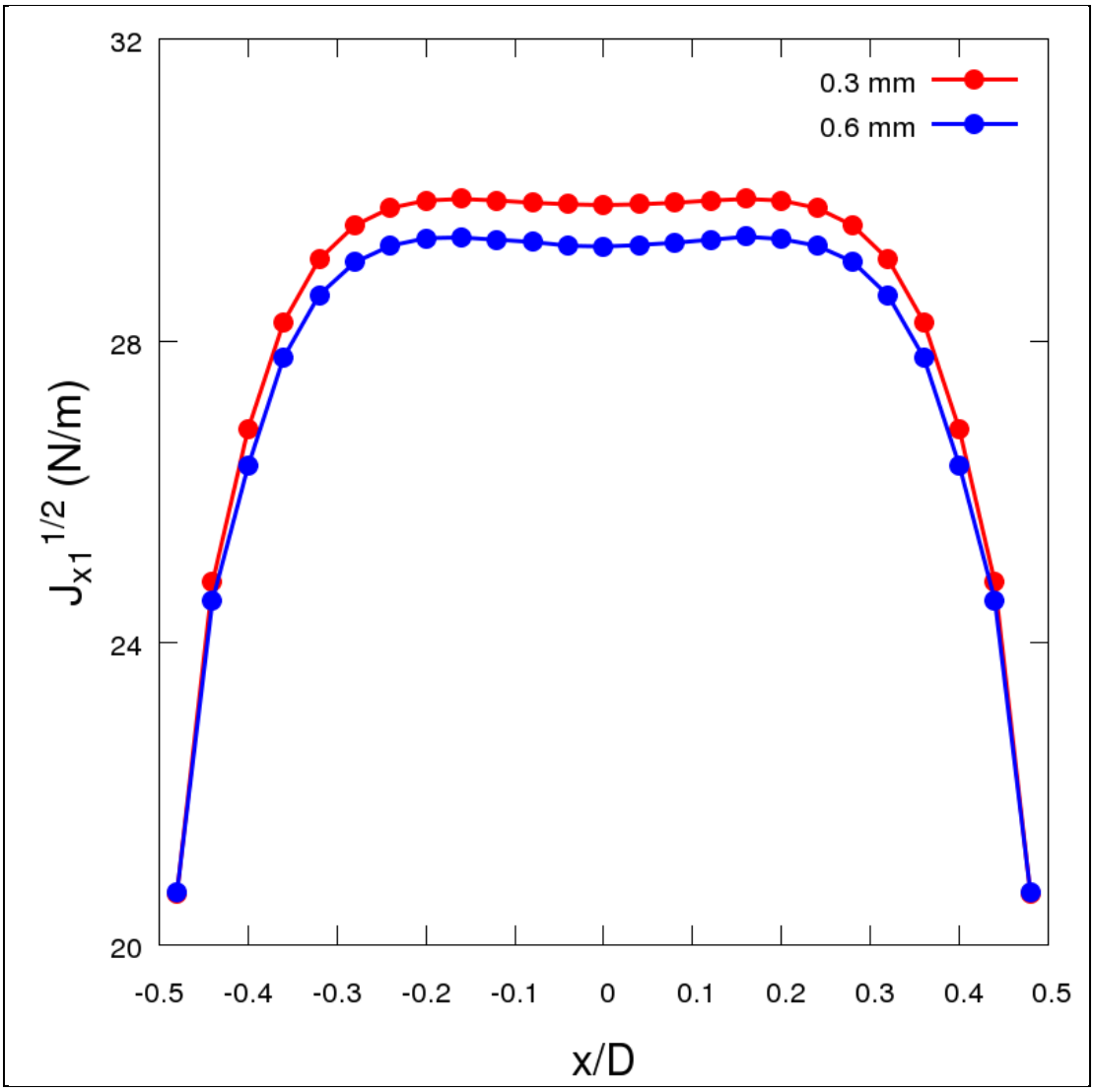

Figure 5. $J_{x1}^{1/2}$ vs. axial coordinate for a platen displacement of 0.3 mm for standard butterfly specimens with mesh resolutions of 0.6 and 0.3 mm.

Experimentally, aluminum platens are likely to be utilized in a SHPB setup due to their lower impedance, which is important to obtain a high signal strength in the dynamic experiments. Simulations substituting aluminum (E = 68.9 GPa; ν = 0.33) platens gave no appreciable differences from those of steel platens.

3.2 Friction and Specimen Thickness Effects

The effects of friction were analyzed by loading the standard specimen with steel platens; the lower platen was held fixed while the upper platen was given a fixed velocity of 1 m/s. Friction was modeled with a fixed Coulomb friction coefficient between the epoxy and steel ranging between 0.01 and 1. Initial investigation of the standard specimen revealed a nonlinear dependence between J_{x1} at a given platen displacement and the friction coefficient. Further

investigation demonstrated that the specimen thickness D and the friction coefficient combined to give a complicated effect on J_{x1}. Figure 6 shows $J_{x1}^{1/2}$ on the center-plane of the specimen vs. the friction coefficient for specimen thicknesses of 5, 10, 20, 25, and 40 mm, at a platen displacement of 0.3 mm. Even when renormalizing the specimens to a common

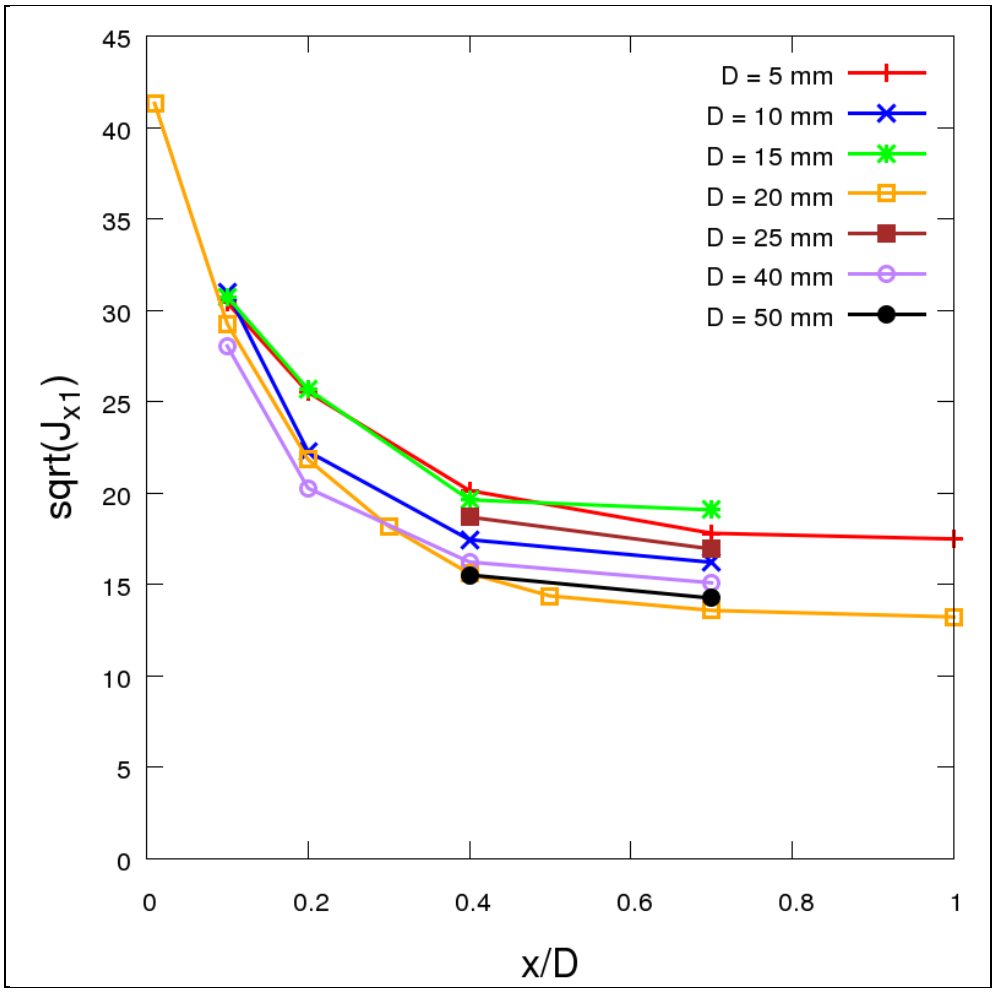

Figure 6. Square root of J_{x1} at the center-plane vs. friction coefficient for several specimen thicknesses.

load-per-unit-length, the results were difficult to interpret. Careful examination of the simulation data revealed that the displacement difference between the lower and upper tips of the specimen ($\delta_2 - \delta_1$) was a more direct indication of the actual load state of the crack-tip. This observation is not entirely surprising; the displacement difference is directly related to the bending moment applied to the specimen and, thus, the load at the tip. Figure 7 shows $J_{x1}^{1/2}$ at the specimen center-plane as a function of the tip displacement difference for various platen displacements (0.1 to 0.6 mm), specimen thicknesses (5 to 50 mm), and friction coefficients (0.01 to 1.0). Note the excellent linear correlation ($R^2 > 0.99$) between the tip displacement difference and $J_{x1}^{1/2}$.

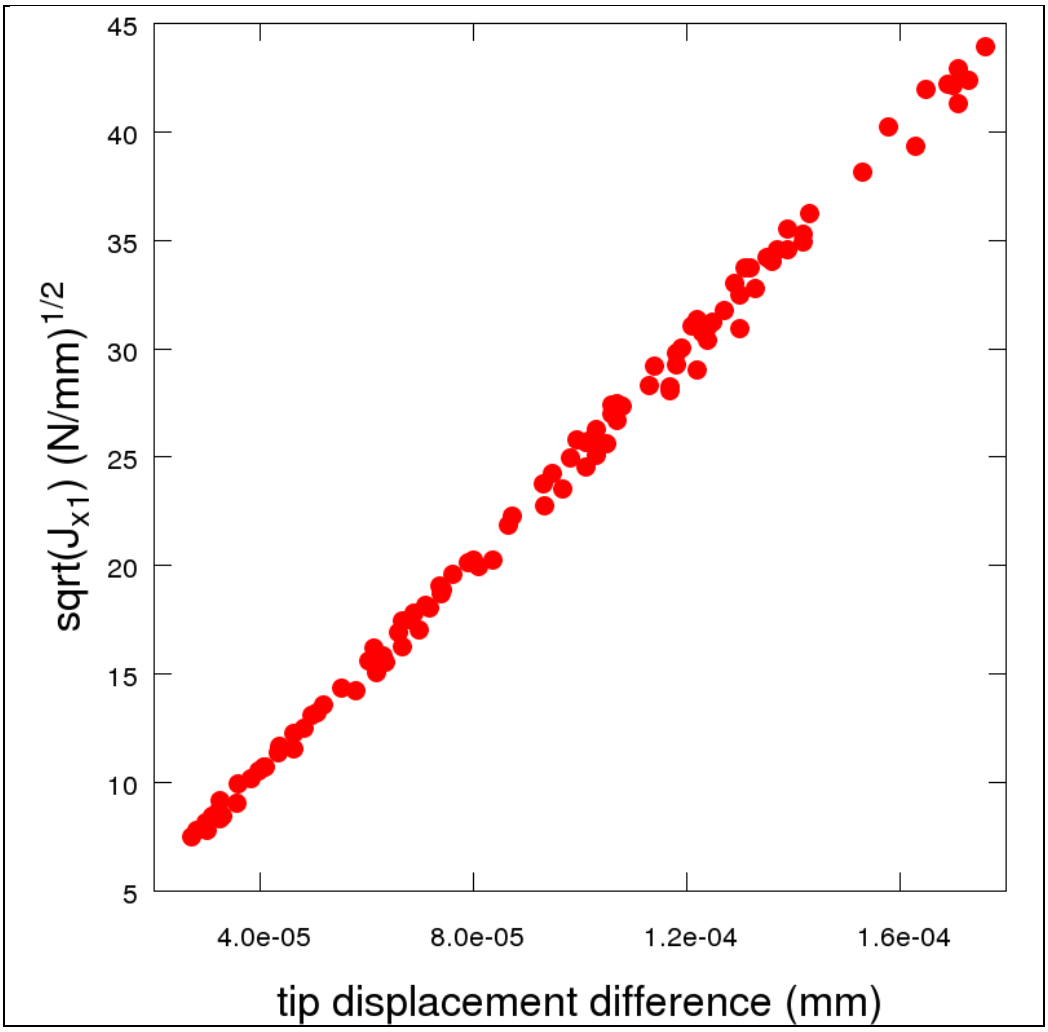

Figure 7. Square root of J_{x1} at the center-plane for various specimen thicknesses, friction coefficients, and platen displacements.

Specimen thickness is an important consideration when analyzing the data from the simulations. Figure 8 shows J_{x1} as a function of axial position in the specimen, for several different specimen thicknesses, for a friction coefficient of 0.7. Note that there is a marked difference between the thin (e.g., 5 mm) and the thicker (e.g., 40 mm) specimens; this is similar to the plane stress to plane strain transition seen in the edge-cracked specimens in section 3.1. The overshoot near the edges of the thicker specimens appears to be a frictional effect—their magnitude is reduced greatly for low values of the friction coefficient. Looking at the center-plane of the specimens, there is a clear transition from plane-stress for thinner specimens to plane strain for the thicker ones. Partitioning the data in figure 7 into thin (<20 mm), transitional (20–25 mm), and thick (>25 mm) specimens gives figure 9, where one can observe two distinct linear correlations with $R^2 > 0.999$. For a given tip displacement difference, the thick correlation ranges from 4.45% to 5.1% less than the thin correlation, comparing well with the 4.61% predicted for the plane strain to plane stress ratio.

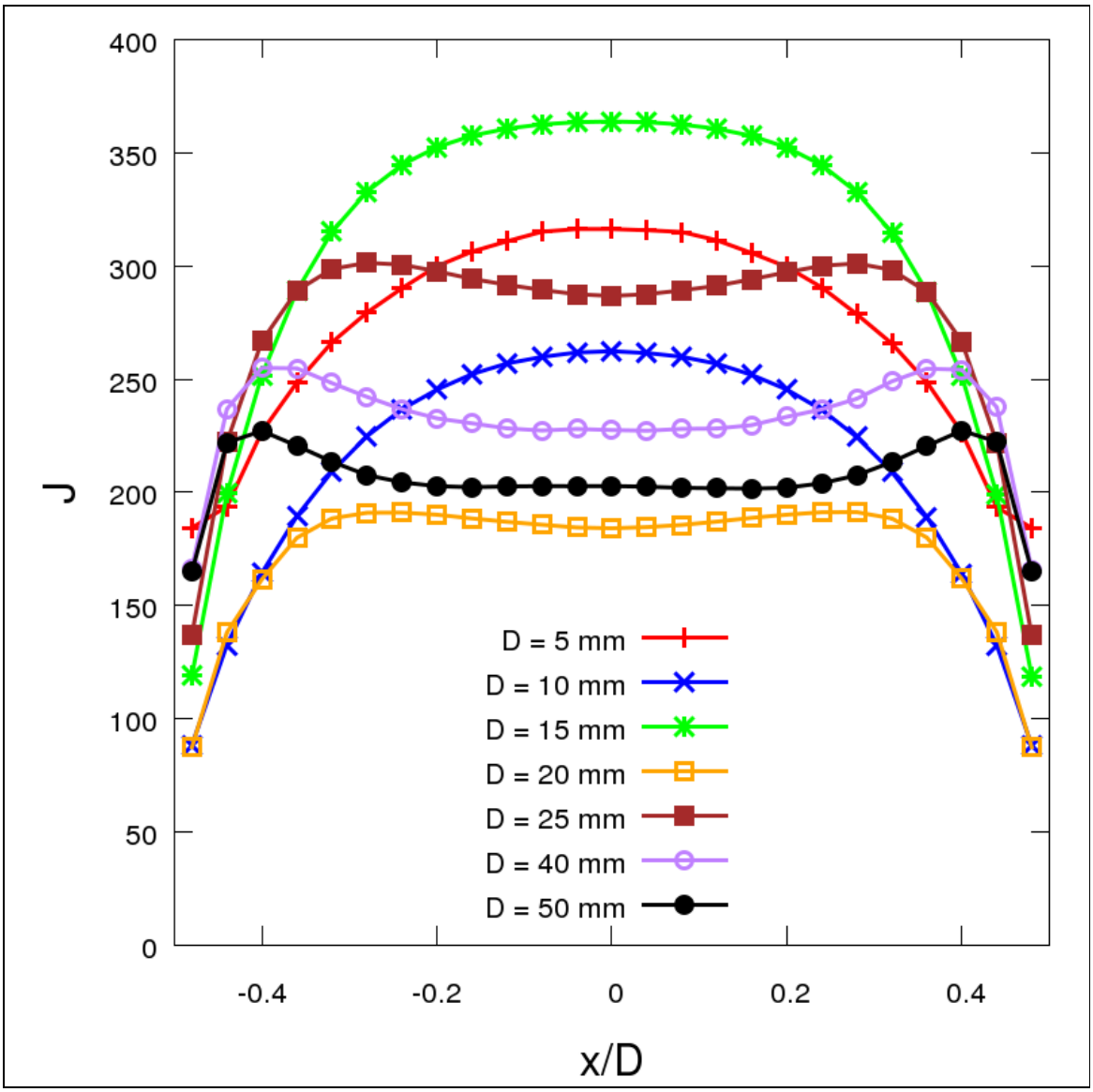

Figure 8. J_{x1} vs. axial position for butterfly specimens of various thicknesses.

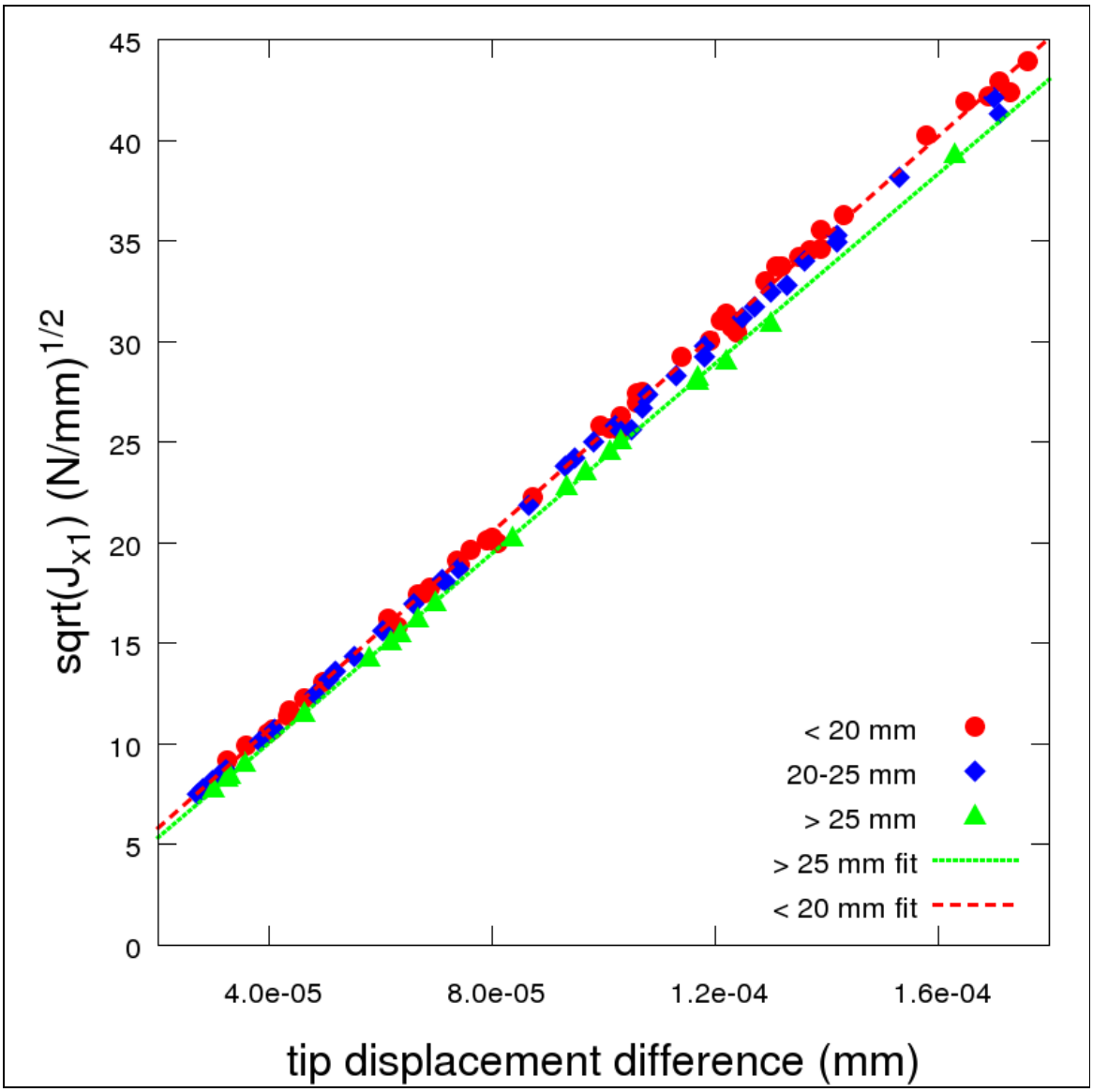

Figure 9. Square root of J_{x1} at the center-plane for various specimen thicknesses, friction coefficients, and platen displacements; data separated into thin (< 20 mm), thick (> 25 mm), and transitional (20–25 mm) sets.

3.3 Butterfly Specimen Geometry

In order to generate a stress intensity factor function for a generalized butterfly specimen, a large number of analyses were conducted utilizing a plane strain formulation and rigid platens with a constant friction coefficient ($\mu = 0.4$). These assumptions were made for convenience; the discovery of the tip displacements as an effective load (section 3.2) reduced the impact of such assumptions, and the significantly smaller computational load of a plane strain problem allowed a large number of analyses to be conducted to compute and verify the geometric factors.

The stress intensity factor was assumed to have the general form of

$$K_I = \frac{6M\sqrt{\pi a}}{(1-\alpha)^{3/2} H} f(\alpha) g(...), \tag{7}$$

where M represents the moment (or here tip displacement differential) and $f(\alpha)$ and $g(\ldots)$ represent functions of nondimensional parameters that characterize the specimen geometry. This functional form is taken from commonly published forms for the stress intensity factor for four-point bending specimens (*8*).

Four nondimensional parameters were selected to parameterize the geometry: $\alpha = a/H$ represents the relative crack length, L_2/L_1 and H/L_1 represent geometric factors for the applied moment, and a_0/H represents the depth of the wide V at the base of the specimen. There are some obvious geometric restrictions ($\alpha > a_0/H$, $L_2/L_1 > 1$, and $H/L_1 > 2$), but practical considerations and initial numerical trials revealed realistic ranges for the nondimensional parameters. The crack length a must be less than $H - L_1$ (geometrically), but in practice the parameter α should be in the range $0.2 < \alpha < 0.5$; values outside of this range see crack-tip stress-fields affected by the contact stress-fields. The spread ratio L_2/L_1 and height ratio H/L_1 have an interdependent relationship for practical bounds. Small spread ratios and large height ratios result in a near-uniaxial compression test rather than the desired four-point-bending-like test; practically, L_2/L_1 must be greater than 1.75 and H/L_1 must be less than 12. The ratio $(L_2-L_1)/H$ is a better indicator of this effect. Bounding this ratio by $0.1 < (L_2-L_1)/H < 0.5$ prevents both compression effects and the specimen lateral surfaces from affecting the crack-tip stress field. The base V ratio a_0/H was found to have little effect on results as long as it was appreciably less than α ($a_0/H < 0.7\alpha$ gave good results); values of a_0/H approaching α unsurprisingly gave results resembling a V-notch rather than a sharp crack.

Initial simulations were conducted with a base geometry of $L_1 = 2$ mm, $L_2/L_1 = 3$, $H/L_1 = 8$, and $a_0/H = 2/3*\alpha$, with variable α to ascertain the effects of α on the stress intensity factor. Figure 10 shows the simulation results of a sweep of $0.2 \le \alpha \le 0.4$, normalized by the tip displacement difference and the factor in equation 7. The fit shown in figure 10 is of the form

$$f(\alpha) = Ce^{A(1-\alpha)}, \tag{8}$$

where, for this case, $C = 0.005912$ and $A = 7.3045$. The accuracy of the fit is excellent, with $R^2 > 0.999$.

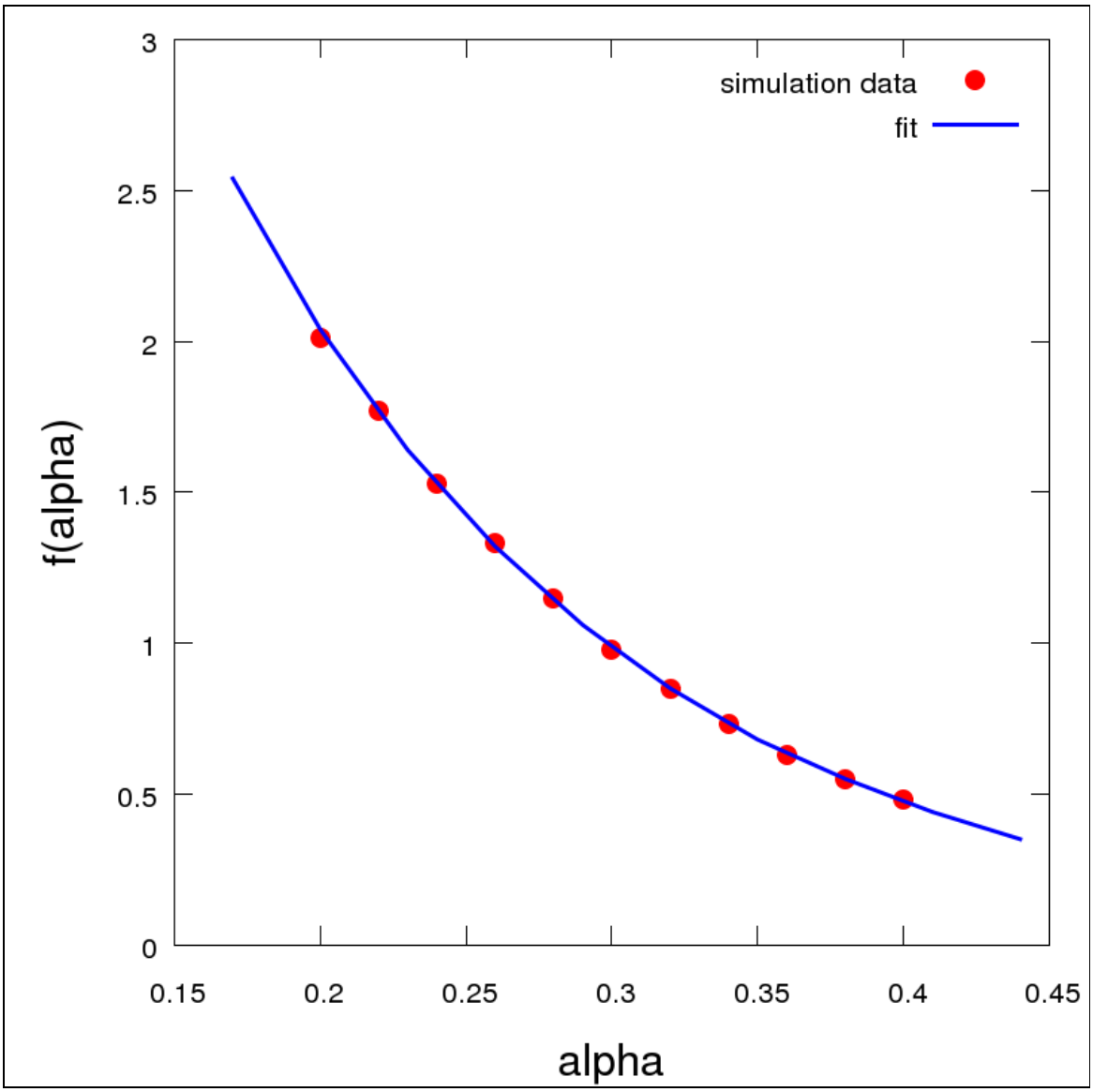

Figure 10. Normalized stress intensity factor vs. α for L_2/L_1 = 3 and H/L_1 = 8.

To explore the other geometric effects, α was held constant at 0.3 and L_2/L_1 and H/L_1 were varied over the ranges $2 < L_2/L_1 < 3.5$ and $6 < H/L_1 < 12$. Unlike previous studies, where tip displacement difference was the best indicator of loading, it was found that the fit for the stress intensity factor was more accurate with a moment description of

$$M \propto \frac{\delta_2 L_2 - \delta_1 L_1}{H}, \tag{9}$$

where δ_2 *and* δ_1 *are the displacements of the lower and upper tip, respectively.* Note that for a constant L_2/L_1, this simply reduces to the displacement difference and all previous results hold.

Further experimentation with parametric functions found that a single function of $(L_2\text{-}L_1)/H$ yielded acceptable accuracy, as shown in figure 11. The functional fit chosen is of the form

$$g\left(\frac{L_2 - L_1}{H}\right) = C(1 - B\left(\frac{L_2 - L_1}{H}\right)), \tag{10}$$

where C = 1.3173 and B = 1.1093. The fit prediction was ±5% for all simulated points. Much of this error is likely attributable to contact patch discretization differences, as the scatter of a set of analyses with identical geometry, but a slightly different local discretization, is on this order of magnitude.

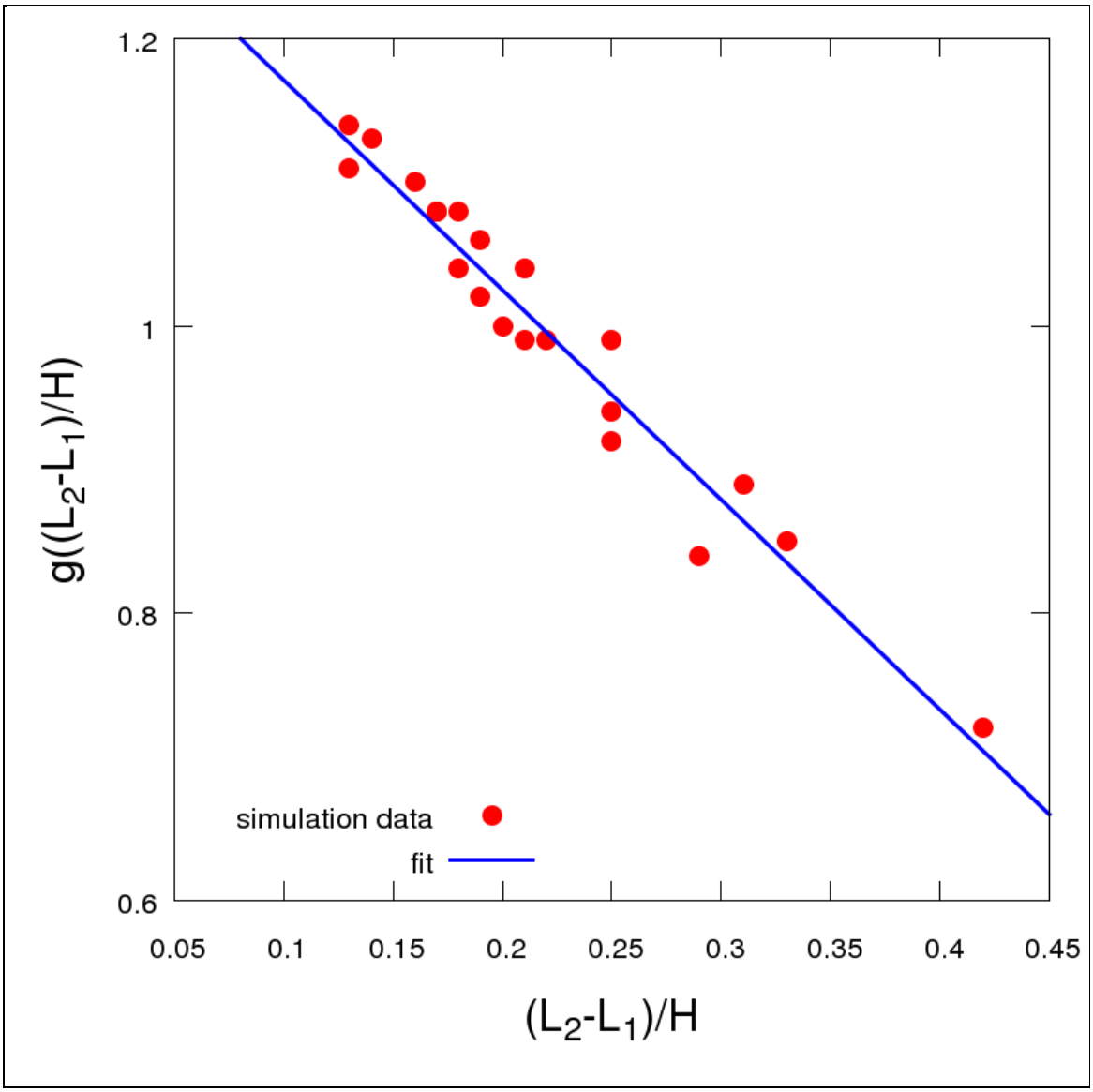

Figure 11. Normalized stress intensity factor vs. $(L_2\text{-}L_1)/H$.

Putting equations 7, 8, and 10 into a single function gives

$$K_I = C\frac{6M\sqrt{\pi a}}{(1-\alpha)^{3/2}H}e^{A(1-\alpha)}\left(1-B\left(\frac{L_2-L_1}{H}\right)\right), \tag{11}$$

where the moment is defined as

$$M = E'D^2\frac{\delta_2 L_2 - \delta_1 L_1}{H}. \tag{12}$$

The E' in equation 12 is E (Young's modulus) for plane stress or $E/(1-\nu^2)$ for plane strain. The specimen thickness D is taken to be 1 for 2-D analyses. The constants in the equation are $A = 7.3045$, $B = 1.1093$, and $C = 2.871 \times 10^{-8}$. The overall error in this equation is bounded by ±5%, much of which is numerical setup dependent (when comparing with computed results).

3.4 Crack Width and Shape Effects

The crack width and crack tip shape (from α to α_0) were held constant with a semicircular crack-tip and a crack width of $w_c = 0.3$ mm for all of the analyses carried out previously. The $\alpha = 0.3$, $L_2/L_1 = 3$, $H/L_1 = 8$ geometry was simulated with several crack configurations: (1) crack width of 0.3 mm with a round crack-tip, (2) crack width of 0.15 mm with a round crack-tip, and (3) a perfect "crack" with zero width and a sharp crack-tip. The results in these three cases varied by a maximum of 2.1% (the comparison of the sharp crack with the widest notch), indicating that this effect is small for reasonable values of crack width. Similarly, for a constant width notch with V, semicircular, and square notch tips, the difference was 1.3%, indicating that measuring the exact depth of the notch is more critical than the exact notch shape.

3.5 Validation

To validate the model, a random number generator was utilized to generate four random numbers to describe the geometry within the bounds 1 mm < L_1 < 4 mm, 0.2 < α < 0.4, 2 < L_1/L_2 < 3.5, and 6 < H/L_1 < 12. Crack widths were held to be a constant 0.3 mm with a semicircular crack-tip. Simulations were conducted for each of the geometries and compared with the analytical model. Results are shown in table 2. Note that all errors are less than 7%, with three of four cases less than 3.5%. The small α of case 2 likely causes the larger error; this value is at the extremum of the calibrated function for $f(\alpha)$.

Table 2. Comparison of analytical and numerical result for validation geometries.

Case No.	L_1 (mm)	α	L_2/L_1	H/L_1	$J_{x1}^{1/2}$ (simulation) ((N.m)$^{1/2}$)	$J_{x1}^{1/2}$ (analytical) ((N.m)$^{1/2}$)	Error (%)
1	2.982	0.2377	2.3782	7.1056	21.42	20.79	–2.94
2	3.498	0.2015	2.6785	9.0660	12.57	11.73	–6.69
3	3.020	0.2734	2.8663	6.1108	27.79	28.71	3.33
4	2.215	0.3340	2.0311	8.1312	16.45	16.26	–1.11

4. Discussion

The stress intensity factor function given by equation 11 gives a reasonably accurate prediction for a linear elastic, brittle material under idealized (2-D) loading. The use of contact patch displacements allows variability in friction coefficients to be accounted for in a straightforward way with established DIC techniques that are already a part of the instrumentation suite (*2*). For brittle materials, such as the epoxies in Whittie et al. (*2*), equation 11 should provide a reasonable estimate of the stress intensity factor at the crack-tip for quasi-statically loaded butterfly specimens. One possible use of this work is to design specimen geometries tailored to the properties of new epoxies (stiffness, strength, fracture toughness, etc.).

The analysis in this work has some limitations. The linear elastic constitutive relation is, of course, a simplification. Obvious ramifications are the lack of rate effects (strain-rate hardening, viscoelasticity, and fracture energy as a function of rate), but it also eliminates local yielding from the analysis. This fact should be considered when designing specimens, as the local stresses from the small contact patches can be quite large, leading to yielding at the contact points before fracture begins. Yielding can also occur at the crack-tip before fracture begins, although typical plastic-zone techniques developed in the fracture mechanics community can compensate for this yielding. Note that while the finite element analysis includes inertia, the loading pulses are long and well conditioned. When conducting dynamic analyses, care must be taken to give the specimen monotonic loading (e.g., through the use of pulse shaping on the SHPB), as vibrational modes of the specimen can be excited under other loading types, leading to hard-to-interpret results.

Future extensions of this work will include rate-dependent effects in both the material constitutive behavior and the fracture toughness of the material, and application of similar analysis for the use of the ARL butterfly geometry to study the fracture behavior in adhesive bonds. Whittie et al. (*2*) noted that the fracture energy nominally doubled when the loading rate was increased from 7 to 70 kN/s. Whether this change in fracture energy is a result of strain-rate hardening, viscoelasticity, or rate dependency of fracture energy remains to be seen.

5. References

1. Syn, C. J.; Chen, W. W. Surface Morphology Effects on High-Rate Fracture of an Aluminum/Epoxy Interface. *Journal of Composite Materials* **2008**, *42*, 1639–1658.
2. Whittie, S.; Moy, P.; Gunnarson, C. A.; Knorr, D.; Weerasooriya, T.; Lenhart, J. Fracture Response of Cross-Linked Epoxy Resins as a Function of Loading Rate. In *Proceedings of the Society of Experimental Mechanics International Conference and Exposition on Experimental and Applied Mechanics*, Costa Mesa, CA, 11–12 June 2012; The Society for Experimental Mechanics: Bethel, CT.
3. Weerasooriya, T.; Gunnarson, C. A.; Jensen, R.; Chen, W. Strength and Failure Energy for Adhesive Interfaces as a Function of Loading Rate. In *Dynamic Behavior of Materials, Volume 1, Conference Proceedings of the Society For Experimental Mechanics Series 99*; Proulx, T., Ed.; DOI 10.1007/978-1-4614-0216-9_9; The Society for Experimental Mechanics: Bethel, CT, 2011.
4. Sandia National Laboratories. *Sierra/Solid Mechanics 4.22 User's Guide;* SAND2011-7597; Albuquerque, NM, 2011.
5. Li, F. Z.; Shih, C. F.; Needleman, A. A Comparison of Methods for Calculating Energy Release Rates. *Engineering Fracture Mechanics* **1985**, *21*, 405–421.
6. Rice, J. R. A Path Independent Integral and the Approximate Analysis of Strain Concentration by Notches and Cracks. *Journal of Applied Mechanics* **1968**, *35*, 379–386.
7. Carka, D.; Landis, C. M. On the Path Dependence of the J-Integral Near a Stationary Crack in an Elastic-Plastic Material. *Journal of Applied Mechanics* **2011**, *78*, 1–6.
8. Tada, H.; Paris, P. C.; Irwin, G. R. *The Stress Analysis of Cracks Handbook*; 3rd ed.; American Society of Mechanical Engineering Press: New York, 2000.
9. Giner, E.; Fernández-Zúñiga, D.; Fernández-Sáez, J.; Fernández-Canteli, A. On the Jx1-Integral and the Out-of-Plane Constraint in a 3-D Elastic Cracked Plate Loaded in Tension. *International Journal of Solids and Structures* **2010**, *47*, 934–946.

NO. OF COPIES	ORGANIZATION
1 (PDF only)	DEFENSE TECHNICAL INFORMATION CTR DTIC OCA 8725 JOHN J KINGMAN RD STE 0944 FORT BELVOIR VA 22060-6218
1	DIRECTOR US ARMY RESEARCH LAB IMAL HRA 2800 POWDER MILL RD ADELPHI MD 20783-1197
1	DIRECTOR US ARMY RESEARCH LAB RDRL CIO LL 2800 POWDER MILL RD ADELPHI MD 20783-1197

NO. OF
COPIES ORGANIZATION

ABERDEEN PROVING GROUND

6 DIR USARL
RDRL WMM B
R CARTER
M FOSTER
B LOVE
P MOY
RDRL WMP B
C HOPPEL
T WEERASOORIYA

INTENTIONALLY LEFT BLANK.